Electronic Supplementary Material (ESI) for Journal of Materials Chemistry A.

Supporting Information

Lithium Metal Batteries with In-Situ Copolymerized Fluorinated Polyether Electrolytes†

Zhichun Chen, Ji Xian, Xiaobo Pan,* Fangping Ren, Yuju Li, Yan Tan, Yunfei Bai, Jincai Wu*

State Key Laboratory of Applied Organic Chemistry (Lanzhou University)

Key Laboratory of Nonferrous Metal Chemistry and Resources Utilization of Gansu Province

College of Chemistry and Chemical Engineering, Lanzhou University

Lanzhou 730000, China

***Corresponding authors**

Email: boxb@lzu.edu.cn; orcid.org/0000-0002-5757-2339

wujc@lzu.edu.cn; orcid.org/0000-0002-8233-2863

Supplementary Figures and tables

Preparation and characterization of electrolytes

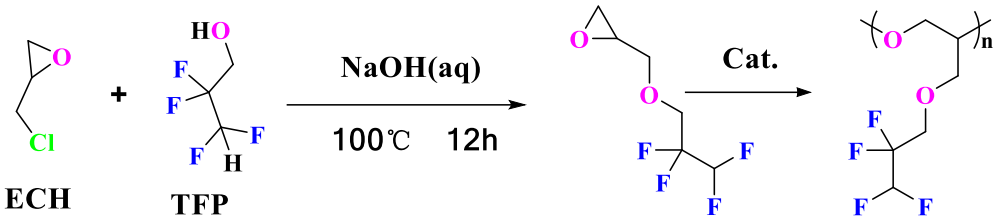

Scheme S1. Synthetic and polymerization route of TFPO molecule.

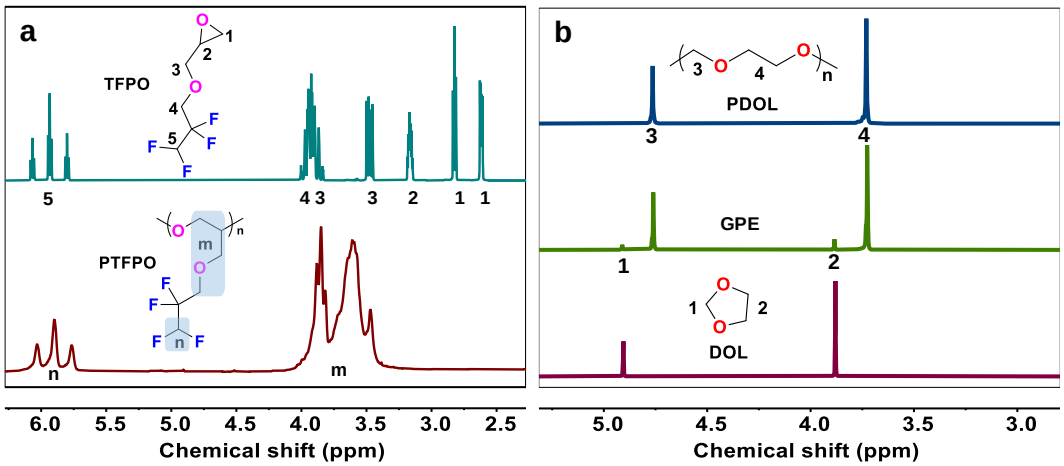

Fig. S1 TFPO and DOL monomers and polymers (^{1}H NMR in $CDCl_3$).

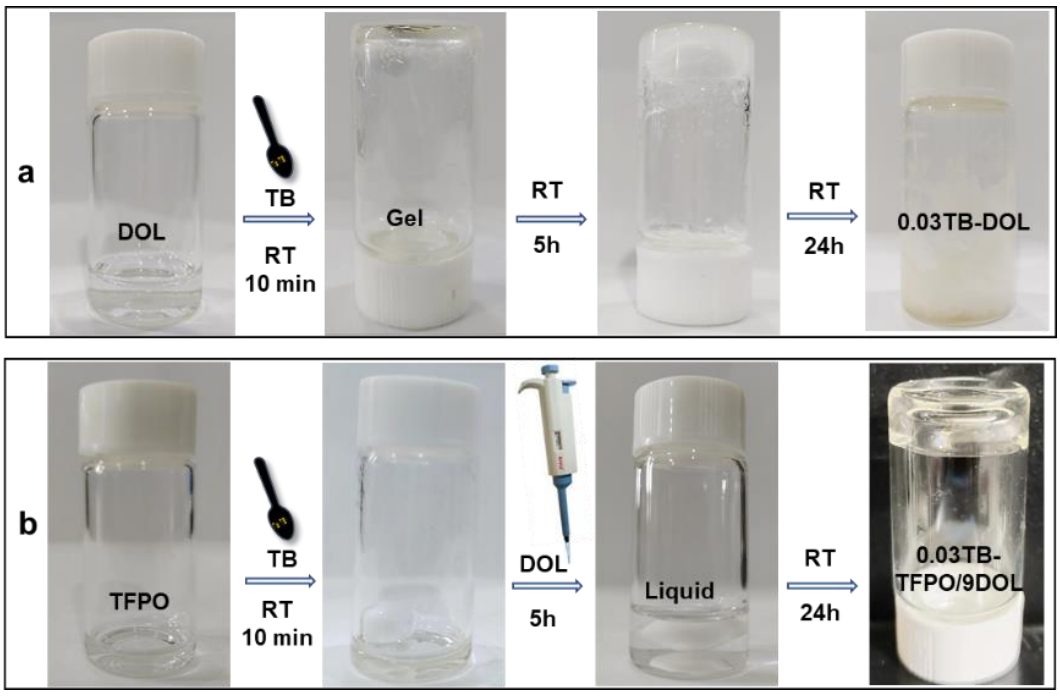

Fig. S2 Changes in the appearance state of (a) 0.03 TB-DOL electrolyte and (b) 0.03 TB-TFPO/9DOL electrolyte after different reaction times. The comparison shows that the introduction of TFPO can reduce the polymerization rate of DOL and is more suitable for in-situ preparation in batteries.

Table S1. Fluorinated polymer electrolytes were prepared by mixing different volume ratios of DOL and TFPO under the following polymerization conditions:

Abbreviation of electrolyte	Monomer (volume ratio) TFPO/DOL	Lithium salt	Initiator	Conditions	Conv. (DOL)
(a) 0.03TB-DOL	0/10	2 M LiTFSI	0.03 M TB	RT 1d	91%
(b) 0.03TB-TFPO/9DOL	1/9	2 M LiTFSI	0.03 M TB	RT 2d	90%
(c) 0.03TB-2TFPO/8DOL	2/9	2 M LiTFSI	0.03 M TB	30 ℃ 2d	88%
(d) 0.03TB-3TFPO/7DOL	3/7	2 M LiTFSI	0.03 M TB	30 ℃ 2d	67%

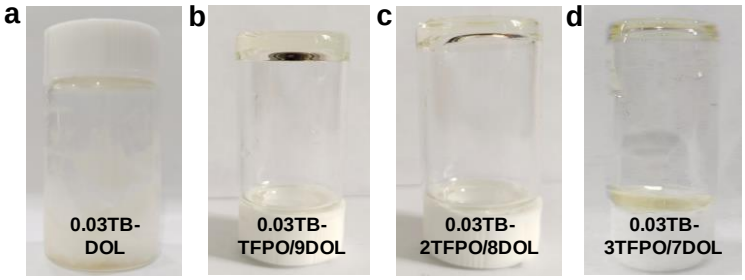

Fig. S3 Appearance status of different polymer electrolytes.

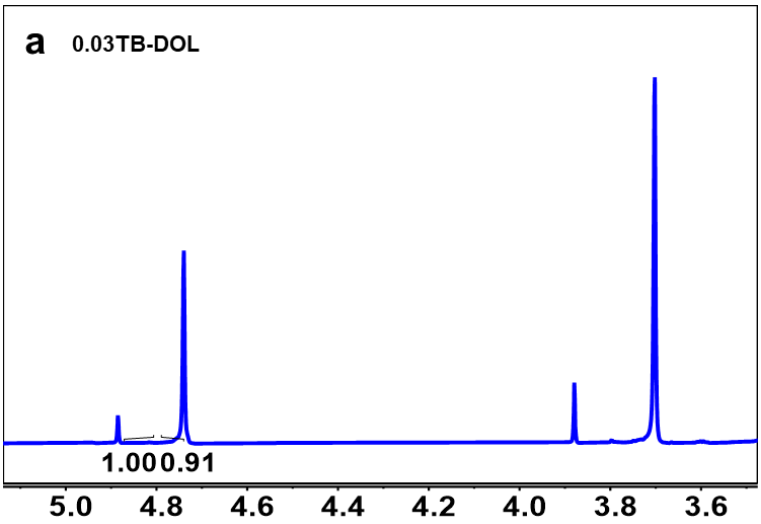

Fig. S4 ^{1}H NMR of the 0.03TB-DOL homopolymerized electrolyte, the integral shows 91% conversion of DOL.

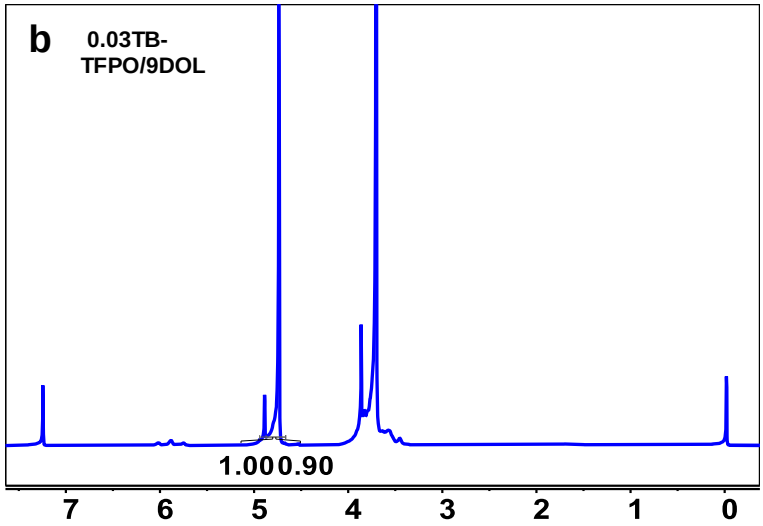

Fig. S5 ^{1}H NMR of the 0.03TB-TFPO/9DOL copolymerized electrolyte, the integral shows 90% conversion of DOL.

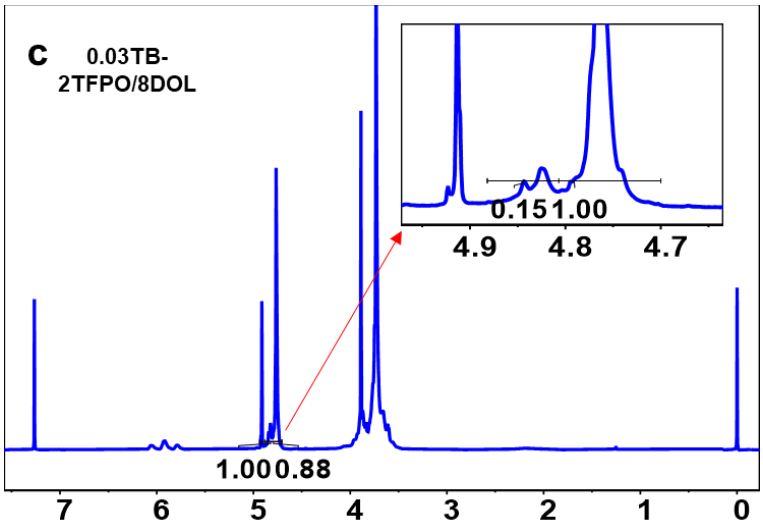

Fig. S6 ^{1}H NMR of the 0.03TB-2TFPO/8DOL copolymerized electrolyte, the integral shows 88% conversion of DOL, the inset shows that copolymer new peak accounts for about 15% of the total polymer.

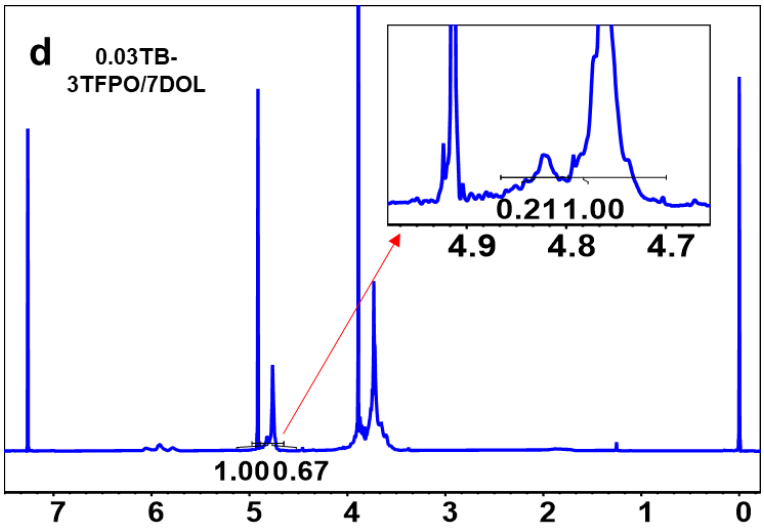

Fig. S7 ^{1}H NMR of the 0.03TB-3TFPO/7DOL copolymerized electrolyte, the integral shows 67% conversion of DOL, the inset shows that copolymer new peak accounts for about 21% of the total polymer.

In the ^{1}H NMR spectra of electrolyte mixtures containing both monomers of DOL and TFPO, except the characteristic peaks of PTFPO and PDOL, the new peaks at 4.8-4.9 ppm should result from the linkage units in the copolymers of DOL and TFPO, the intensities of this new peak increase significantly when the ratio of TFPO and DOL changes from 2/8 to 3/7 (insets of Figure. S5-6, the area of integration of this new peak becomes larger).

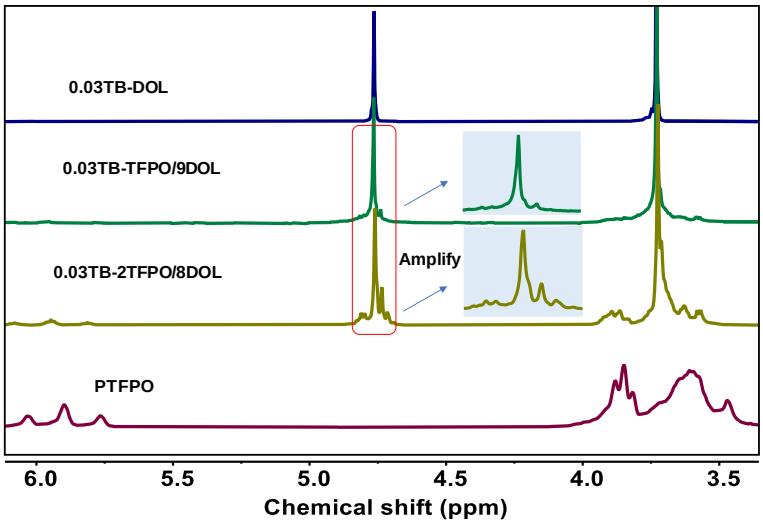

Fig. S8 The ^{1}H NMR of purified polymers. In order to exclude the interference of unpolymerized monomers and impurities, the ^{1}H NMR of different polymers after purification was compared, and it was observed that the new peaks of the polymers were more significant, suggesting that the two monomers had undergone a copolymerization reaction.

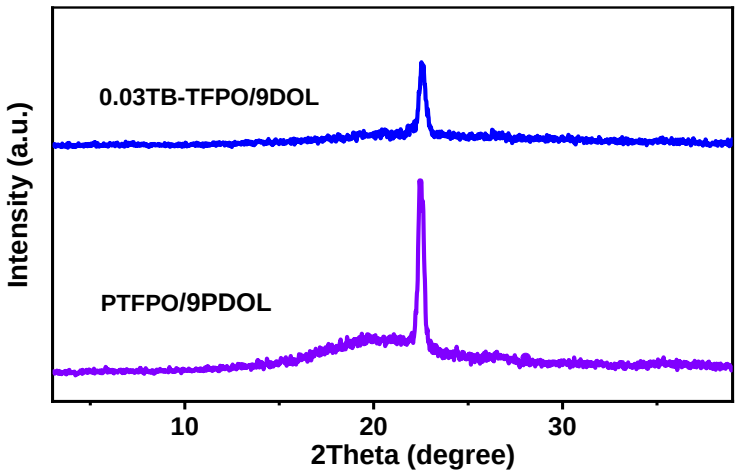

Fig. S9 X-ray diffraction testing of polymers. Compared to homopolymer mixture of 1 equivalent PTFPO and 9 equivalents PDOL, the crystalline degree becomes low for the white purified solid polymer of 0.03TB-TFPO/9DOL.

Electrochemical properties

The Li^+ transfer number was measured by applying a small polarisation potential of 2000 s to the Li-Li symmetric cell to achieve a steady state. The t_{Li^+} was calculated according to the following equation:

$$t_{Li^+} = \frac{I^{SS}R_b^{SS}(\Delta V - I^O R_i^O)}{I^O R_b^O(\Delta V - I^{SS}R_i^{SS})}$$

Lithium-lithium symmetric cell was assembled and then the polarization currents, including the original (I^o) and steady-state (I^{ss}) current values, were recorded under a small polarization potential (ΔV) at 10 mV. Simultaneously, the initial and steady-state values of the bulk resistances (R_b^o and R_b^{ss}) and electrode/electrolyte interfacial resistances (R_i^o and R_i^{ss}) were examined via EISs before and after the potentiostatic polarization.

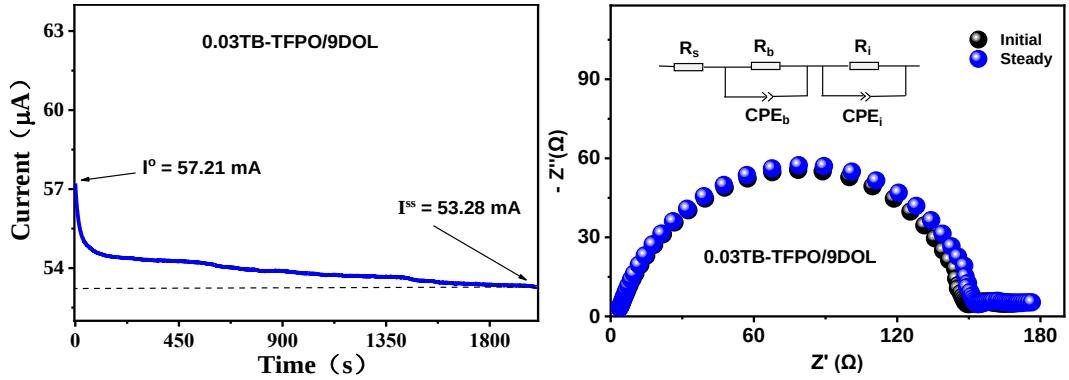

Fig. 10 Lithium-ion transference number measurement of the 0.03TB-TFPO/9DOL electrolyte, potentiostatic polarization (10 mV) curves of electrolyte, electrochemical impedance spectra of electrolyte before and after measurements.

Table S2. The 0.03TB-TFPO/9DOL electrolyte for Li-ion transfer number testing of the corresponding parameters:

DV=0.01V	R_b / Ω	R_i / Ω	I/mA	t_{Li^+}
Initial	2.64	155.31	57.21	-
Steady	2.67	159.02	53.28	0.68

The corresponding parameters obtained from the chronoamperometry curves and electrochemical impedance spectra before and after polarization of the battery, the lithium ion transfer number was calculated from equation to be 0.68.

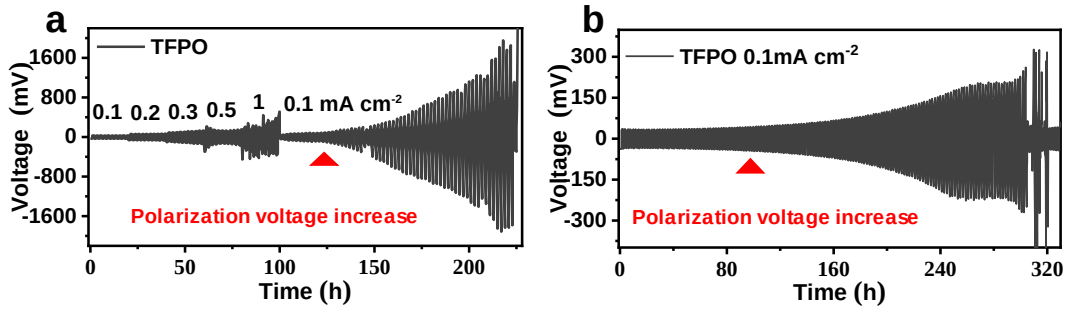

Fig. S11 (a) TFPO deposition/exfoliation cycles at different rates. (b) TFPO deposition/exfoliation cycles at 0.1 mA cm^{-2}.

Analysis of the rate cycling of the symmetric cell containing TFPO electrolyte showed a significant increase in the polarization voltage after about 130 h, the symmetric cell containing a TFPO electrolyte was tested at 0.1 mA cm^{-2} and the cycling curves showed a similar phenomenon.

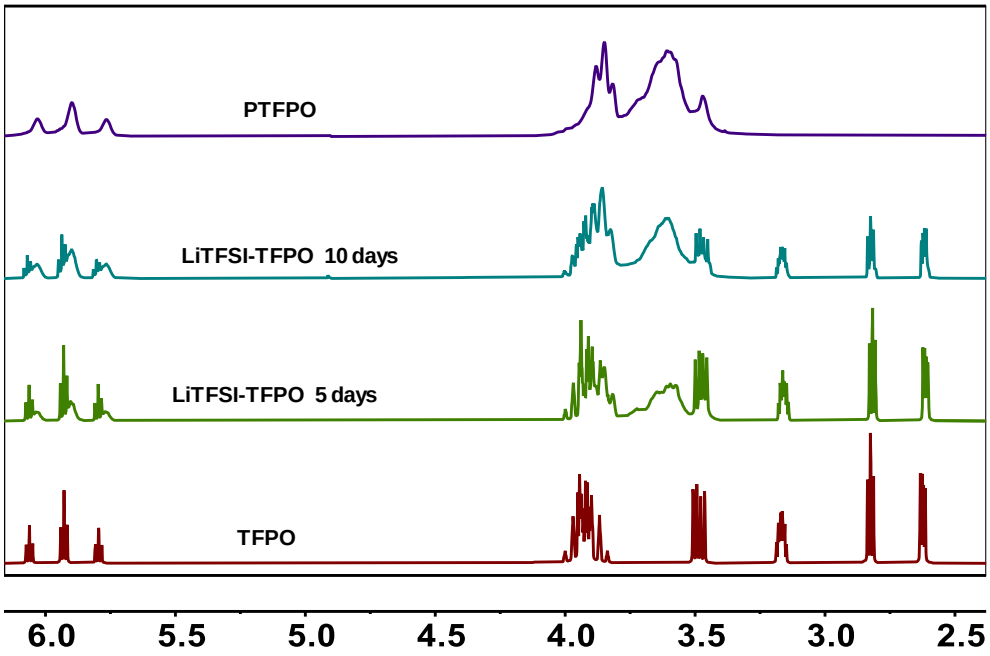

Fig. S12 The ^{1}H NMR comparisons showed that liquid TFPO electrolytes left at room temperature for 5 and 10 days resulted in different degrees of polymerization of TFPO.

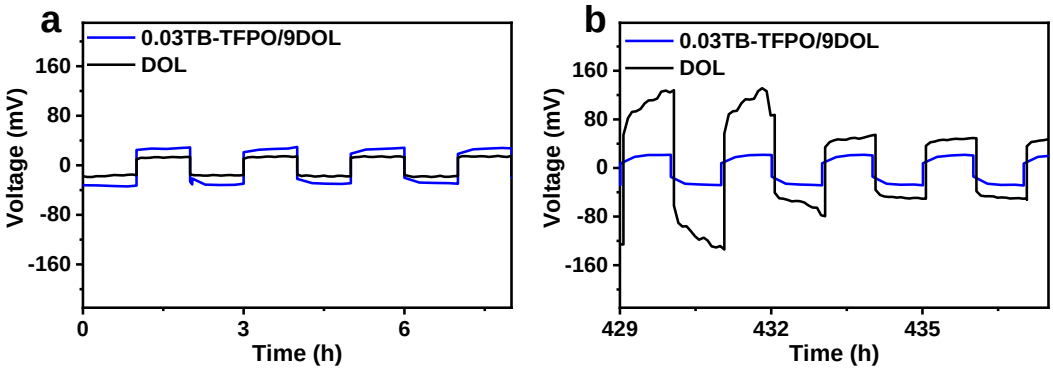

Fig. S13 Local amplification profiles of plating/stripping cycles in lithium-lithium (Li-Li) symmetric batteries containing different electrolytes at 0.1 mA cm^{-2}.

The Nyquist plots of liquid electrolyte batteries display a semicircle at high frequency followed by a tail and are fitted to an equivalent circuit with a resistance and a constant phase element (CPE), ascribed to the bulk resistance (R_b) and the electrode/electrolyte interfacial resistance (R_i), respectively.

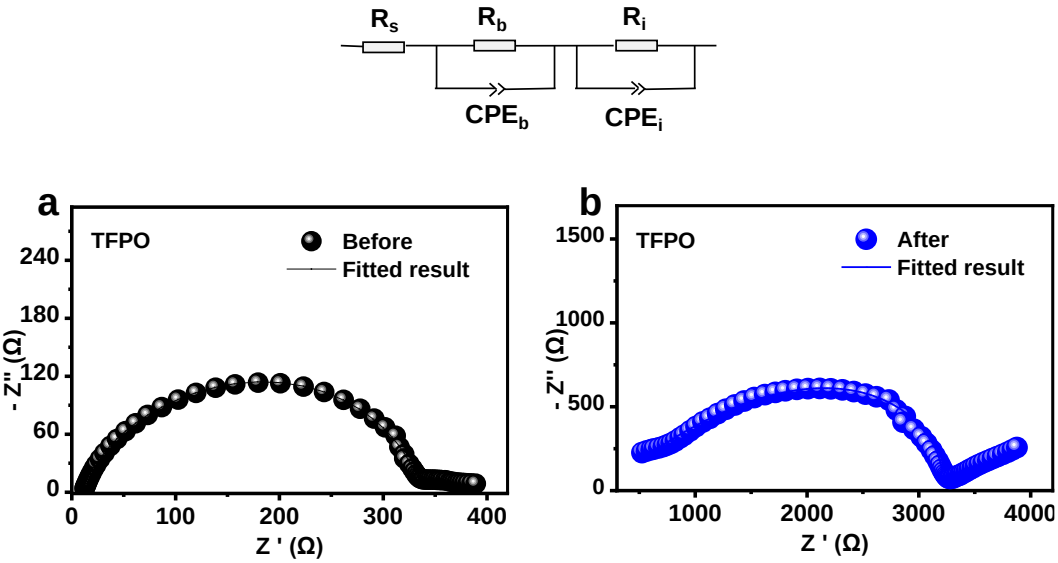

Fig. S14 Changes in electrochemical impedance spectra of Li-Li symmetric batteries with TFPO electrolyte before and after cycling.

Table S3. The EIS fitting results before and after cycling of Li-Li symmetric batteries containing TFPO electrolyte.

TFPO	R_s	R_b/Ω	R_i/Ω
Before	11.6	82.5	243.1
After	106.7	883.9	2367.4

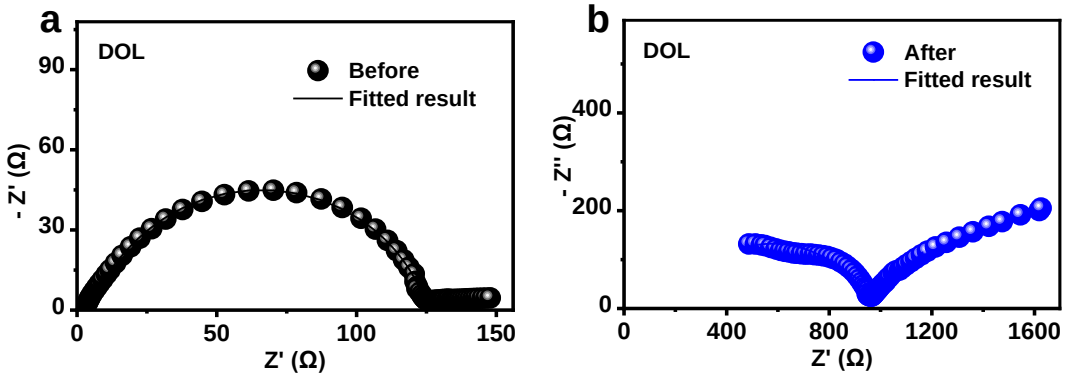

Fig. S15 Changes in electrochemical impedance spectra of Li-Li symmetric batteries with 0.03TB-TFPO/9DOL electrolyte before and after cycling.

Table S4. The EIS fitting results before and after cycling of Li-Li symmetric batteries containing DOL electrolyte.

DOL	R_s	R_b/Ω	R_i/Ω
Before	3.1	3.6	118.7
After	175.2	819.2	1001.2

From the equivalent circuit diagram fitted results, it can be seen that in the liquid electrolyte, both R_b and R_i increase after cell cycling, indicating that both the body and interface resistances become larger, which is consistent with the results of the increase in polarization voltage after cell cycling. Since the EIS of copolymerized electrolyte 0.03TB-TFPO/9DOL has two semicircles, the equivalent circuit diagram is as follows, which increases the circuit element R_{ct} (CPE-R_{ct}) over the equivalent circuit diagram of liquid electrolyte.

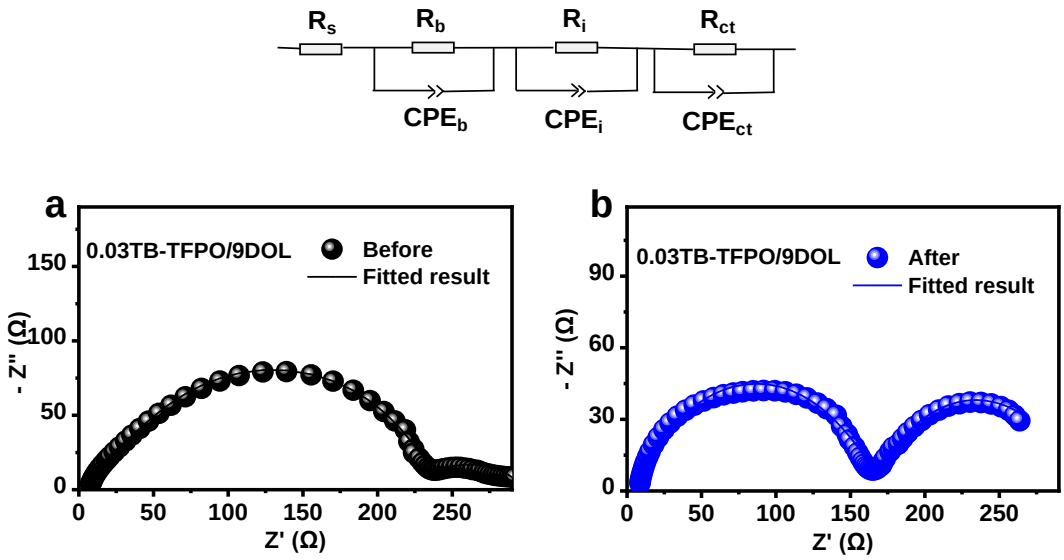

Fig. S16 Changes in electrochemical impedance spectra of Li-Li symmetric batteries with DOL electrolyte before and after cycling.

Table S5. The EIS fitting results before and after cycling of Li-Li symmetric batteries containing 0.03TB-TFPO/9DOL electrolyte.

0.03TB-TFPO/9DOL	R_s	R_b/Ω	R_i/Ω	R_{ct}/Ω
Before	6.9	23.8	200.0	68.6
After	7.9	47.0	106.7	135.0

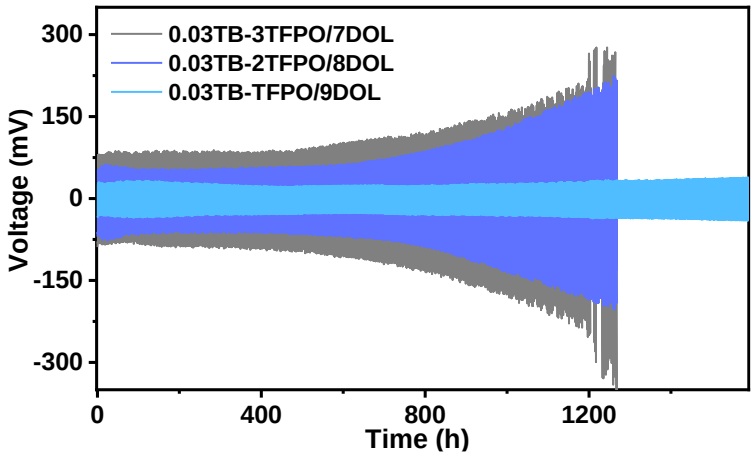

Fig. S17 Plating/stripping cycle life test of Li-Li symmetric batteries with 0.03TB-3TFPO/7DOL, 0.03TB-2TFPO/8DOL and 0.03TB-TFPO/9DOL electrolytes at 0.1mA cm^{-2}.

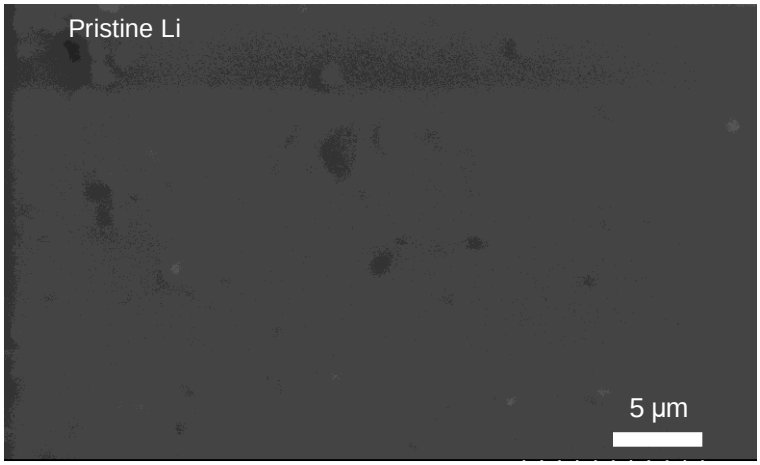

Fig. S18 Scanning electron microscope of pristine lithium-metal surface.

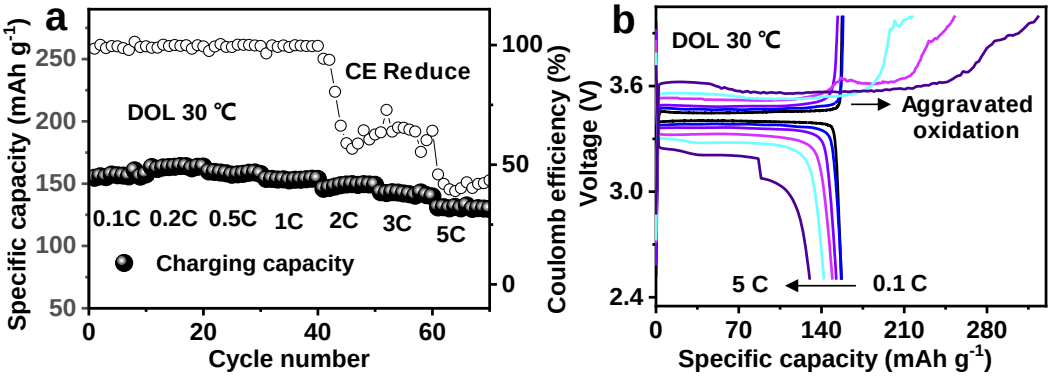

Fig. S19 Li-LFP battery containing DOL electrolyte at 30°C, (a) Rate performance test of current density from 0.1C to 5C. (b) Charge-discharge profiles at different rates.

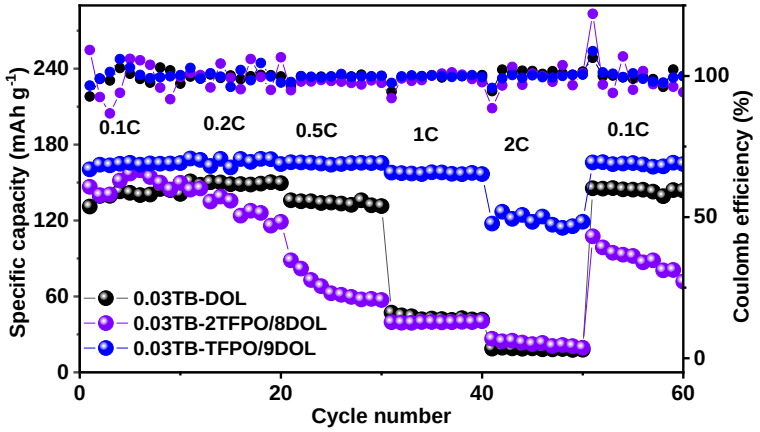

Fig. S20 Rate performance tests of 0.03TB-DOL, 0.03TB-2TFPO/8DOL and 0.03TB-TFPO/9DOL in Li-LFP batteries.

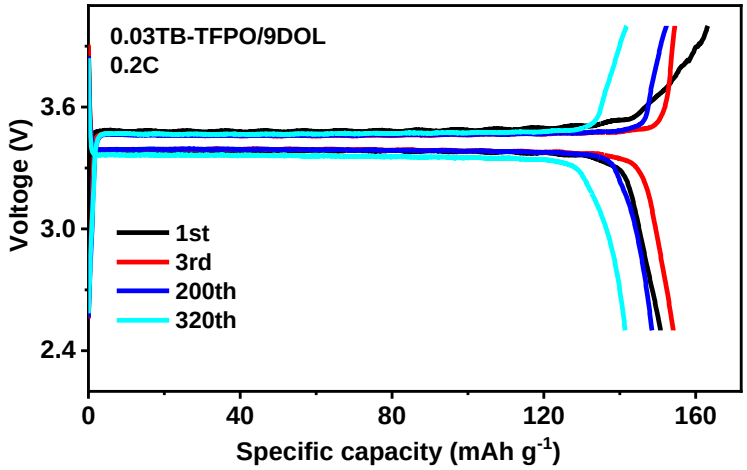

Fig. S21 Charge-discharge profiles of Li-LFP battery containing 0.03TB-TFPO/9DOL electrolyte at a current density of 0.2C.

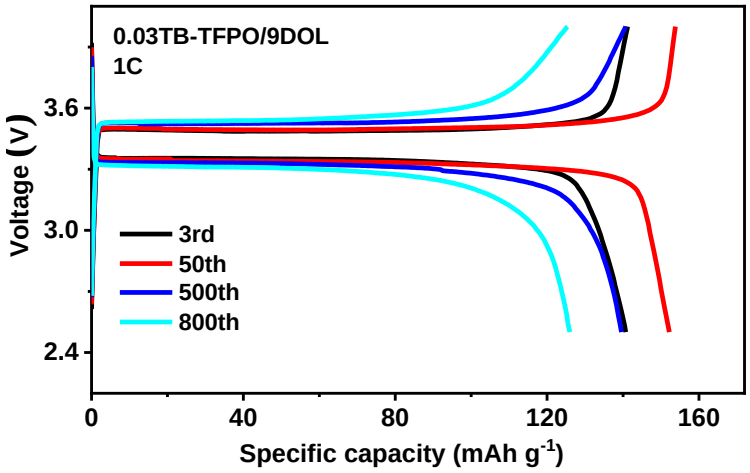

Fig. S22 Charge-discharge profiles of Li-LFP battery containing 0.03TB-TFPO-9DOL electrolyte at a current density of 1C.

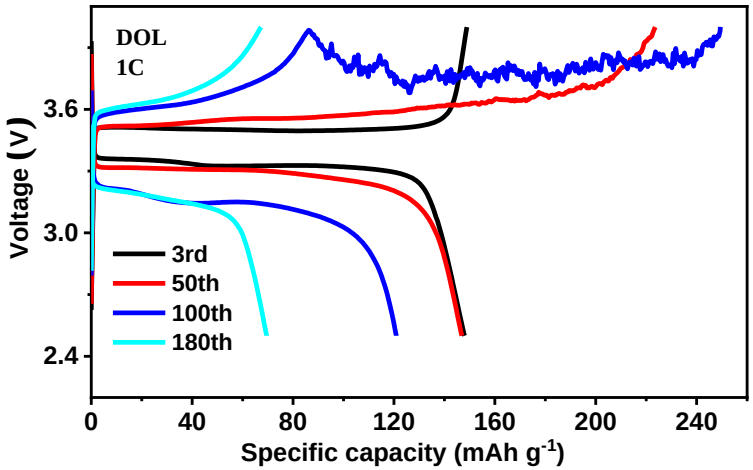

Fig. S23 Charge-discharge profiles of Li-LFP battery containing DOL electrolyte at a current density of 1C.

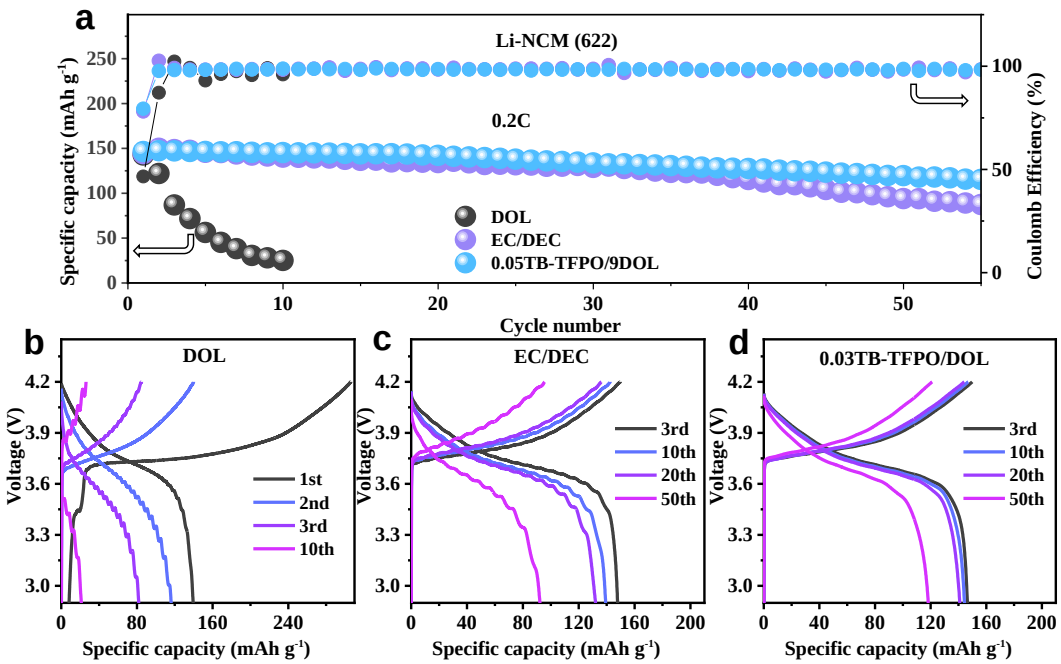

Fig. S24 Performance of different electrolytes in Li-NCM622 batteries. (a) Long cycle of liquid DOL, ester electrolytes (1 M $LiPF_6$ in ethylene carbonate (EC)/diethyl carbonate (DEC) (1/1 by volume)) and 0.03TB-TFPO/9DOL in Li-NCM622 batteries at 0.2 C current density; (b-d) Charge-discharge profiles of Li-NCM622 batteries containing different electrolytes at a current density of 1C.

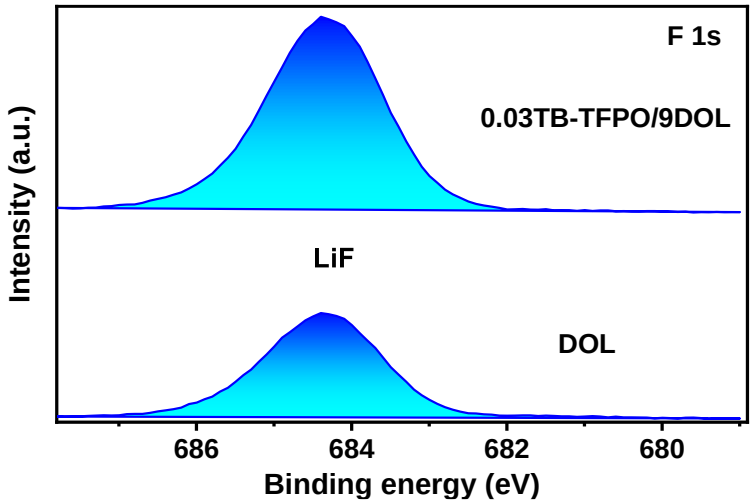

Fig. S25 F 1s spectral analysis was performed on the surface of the LFP electrode after cycling in two electrolytes DOL and 0.03TB-TFPO-9DOL electrolyte.

Table S6. Ionic conductivity and lithium ion transfer number (t_{Li^+}) with reference to different types of blended or copolymerized polymer electrolytes.

Type	Polymer electrolytes	Ionic conductivity [S cm^{-1}]	t_{Li^+}	Ref.
Polymer	PEO	1.90×10^{-6} at 25 °C	-	*Macromolecules*, **2018**[1]
Polymer blend	PMHS/PEO	≈ 10^{-5} at 25 °C	0.31	*Nano Energy*, **2020.**[2]

Copolymer	P(EO-PS)	> 10^{-4} at 60 °C	-	*J. Mater. Chem. A,* ***2016.***[3]
Copolymer	P(EO-PO)	$10^{-5.5}$ at 20 °C	-	*Polymer*, **2001.**[4]
Polymer	PDOL	1.7×10^{-5} at 30 °C	-	*Angew. Chem., Int. Ed.*, **2022.**[5]
In-situ polymerization	PDOL	1.5×10^{-3} at 30 °C	0.58	*Energy Environ. Sci.* **2021.**[6]
Copolymer	TFPO/DOL	5.01×10^{-5} at 40 °C	-	*Angew. Chem., Int. Ed.*, **2022.**[7]
In-situ copolymerization	0.03TB-TFPO/9DOL	1.7×10^{-3} at 25 °C	0.68	This work

Table S7. Reference to oxidation stability, ionic conductivity and batteries cyclic capability for different types of GPEs.

In situ GPE	Initiator Additives	Oxidation Ionic conductivity [S cm^{-1}]	Battery performance	Ref.
PDOL	$LiPF_6$	4.3 V	Li-$LiFePO_4$, 0.5 C, 700 cycles, 95.6 %	Sci. Adv. **2018.**[8]
	DME (50v%)	3.8×10^{-3} at 25 °C		
PDOL	$Al(OTf)_3$	4.7 V	Li–S, 100 cycles, 98%	*Nat. Energy*
	DOL (20v%)	1.1×10^{-3} at 25 °C	Li-$LiFePO_4$, 1 C 700 cycles	**2019.**[9]
PDOL	$LiPF_6$	> 4.9 V	Li-$LiFePO_4$, 0.1 C, 163 mAh/g, 200	*ACS Energy Lett.*
	SiO_2	1.98×10^{-3} at 25 °C	cycles, 99.75%	**2020**.[10]
PDOL	LiDFOB	5 V	Li-$LiFePO_4$, 1C, 1000 cycles, 83.6%	*J. Mater. Chem.*
	SN (wt30%)	3.9×10^{-4} at 25 °C		*A* **2020.**[11]
PTXE	LiDFOB	4.5 V	Li-$LiCoO_2$, 0.3 C, 200 cycles, 88%	*Adv. Sci.* **2020.**[12]
	60% SN	1.14×10^{-4} at 25 °C		
PDOL	TB	4.8 V	Li-S, 0.2 C, 550 cycles, decay rate	*Energy Environ. Sci.* **2021.**[6]
	DOL (20v%)	1.16×10^{-3} at 30°C	0.094%; Li-$LiFePO_4$, 2C, >1200 cycles	
PDOL	$Al(OTf)_3$	4.57 V	Li-$LiFePO_4$, 2 C, 800, 82.5%, 0.2 C, 200	*Adv. Sci.* **2022.**[13]
	PDA/PVDF-HFP	2.39×10^{-3} at 25 °C	cycles, 145.4 mAh/g, 94.8%	
PDOL	$Al(OTf)_3$	4.4 V	Na-NVP, 0.5 C, 100 cycles, 97.1%; 5 C,	*J. Energy Chem.*
	FEC (20v%)	3.31×10^{-3} at 25 °C	98.5 mAh/g, 2000 cycles, 93.6%	**2023.**[14]
PTFPO-DOL	TB	> 4.5 V	Li-$LiFePO_4$, 0.2 C, 320 cycles, 92%; 1C,	This work
	DOL (< 10v%)	1.7×10^{-3} at 25 °C	800 cycles, (90%)	

Table S8. Reference to some fluorinated solvent electrolytes and rate cycling in batteries.

Fluorinated solvent	electrolytes	Oxidation Ionic conductivity [S cm^{-1}]	Battery performance	Ref.
hydrofluoroethers DEG-FTriEG	1 M LiFSA	5.4V 2.7×10^{-4} at 30 °C	Li| NCM 811 0.2 C, >100 cycles	*J. Am. Chem. Soc.* **2020.**[15]

1,4-dimethoxylbutane (FDMB)	1 M LiTFSI/FDMB	>6 V 3.0×10^{-3} at 25 °C	Li|NMC532 0.3 C, 420 cycles, retain 90%	*Nat. Energy* **2020.**[16]
2,2-dimethoxy-4-(trifluoromethyl)-1,3-dioxolane (DTDL)	2 M LiFSI-DTDL	5.5 V 1.4×10^{-3} at 30 °C	Li| NCM 811 0.5 C, 200 cycles, retain 84%	*Nat. Commun.* **2022.**[17]
2-ethoxy-4-(trifluoromethyl)-1,3-dioxolane (cFTOF)	1 M LiFSI-cFTOF	5 V 6×10^{-4} at 25 °C	Li| NCM 811 0.5 C, 110 cycles, retain 100%	*Angew. Chem., Int. Ed.* **2022.**[18]
1,1,2,2-tetrafluoro-3-methoxypropane	1 m LiFSI-TFMP/DME (7v: 1v)	5.8V 2.8×10^{-3} at 25 °C	Cu-NMC811 0.2 C, 100 cycles, retain 87%	*Angew. Chem., Int. Ed.* **2023.**[19]

References

1 S. J. Kwon, B. M. Jung, T. Kim, J. Byun, J. Lee, S. B. Lee and U. H. Choi, *Macromolecules*, 2018, **51**, 10194-10201.
2 C. Sun, Z. Wang, L. Yin, S. Xu, Z. A. Ghazi, Y. Shi, B. An, Z. Sun, H.-M. Cheng and F. Li, *Nano Energy*, 2020, **75**, 104976.
3 L. Long, S. Wang, M. Xiao and Y. Meng, *J. Mater. Chem. A*, 2016, **4**, 10038-10069.
4 P. Jannasch, *Polymer*, 2001, **42** 8629-8635
5 W. Li, J. Gao, H. Tian, X. Li, S. He, J. Li, W. Wang, L. Li, H. Li, J. Qiu and W. Zhou, *Angew. Chem., Int. Ed.*, 2022, **61**, e202114805.
6 J. Xiang, Y. Zhang, B. Zhang, L. Yuan, X. Liu, Z. Cheng, Y. Yang, X. Zhang, Z. Li, Y. Shen, J. Jiang and Y. Huang, *Energy Environ. Sci.*, 2021, **14**, 3510-3521.
7 W. Li, L. Ma, S. Liu, X. Li, J. Gao, S. M. Hao and W. Zhou, *Angew. Chem., Int. Ed.*, 2022, **61**, e202209169.
8 Y.-G. G. Feng-Quan Li, *Sci. Adv.*, 2018, **4**, eaat5383.
9 Q. Zhao, X. Liu, S. Stalin, K. Khan and L. A. Archer, *Nat. Energy*, 2019, **4**, 365-373.
10 P. Yang, X. Gao, X. Tian, C. Shu, Y. Yi, P. Liu, T. Wang, L. Qu, B. Tian, M. Li, W. Tang, B. Yang and J. B. Goodenough, *ACS Energy Lett.*, 2020, **5**, 1681-1688.
11 Q. Liu, B. Cai, S. Li, Q. Yu, F. Lv, F. Kang, Q. Wang and B. Li, *J. Mater. Chem. A*, 2020, **8**, 7197-7204.
12 H. Wu, B. Tang, X. Du, J. Zhang, X. Yu, Y. Wang, J. Ma, Q. Zhou, J. Zhao, S. Dong, G. Xu, J. Zhang, H. Xu, G. Cui and L. Chen, *Adv. Sci.*, 2020, **7**, 2003370.
13 D. Chen, M. Zhu, P. Kang, T. Zhu, H. Yuan, J. Lan, X. Yang and G. Sui, *Adv. Sci.*, 2022, **9**, e2103663.
14 J. Ma, X. Feng, Y. Wu, Y. Wang, P. Liu, K. Shang, H. Jiang, X. Hou, D. Mitlin and H. Xiang, *J.Energy Chem.*, 2023, **77**, 290-299.
15 C. V. Amanchukwu, Z. Yu, X. Kong, J. Qin, Y. Cui and Z. Bao, *J. Am. Chem. Soc.*, 2020, **142**, 7393-7403.
16 Z. Yu, H. Wang, X. Kong, W. Huang, Y. Tsao, D. G. Mackanic, K. Wang, X. Wang, W. Huang, S. Choudhury, Y. Zheng, C. V. Amanchukwu, S. T. Hung, Y. Ma, E. G. Lomeli, J. Qin, Y. Cui and Z. Bao, *Nat. Energy*, 2020, **5**, 526-533.
17 Y. Zhao, T. Zhou, T. Ashirov, M. E. Kazzi, C. Cancellieri, L. P. H. Jeurgens, J. W. Choi and A. Coskun, *Nat. Commun.*, 2022, **13**, 2575.
18 T. Zhou, Y. Zhao, M. El Kazzi, J. W. Choi and A. Coskun, *Angew. Chem., Int. Ed.*, 2022, **61**, e202115884.
19 J. Shi, C. Xu, J. Lai, Z. Li, Y. Zhang, Y. Liu, K. Ding, Y. P. Cai, R. Shang and Q. Zheng, *Angew. Chem., Int. Ed.*, 2023, **62**, e202218151.